Non-invasive methods for assessment of body composition

By M. A. FOSTER and P. A. FOWLER, *Department of Bio-Medical Physics and Bio-Engineering, University of Aberdeen, Foresterhill, Aberdeen AB9 2ZD* and M. F. FULLER, *Rowett Research Institute, Bucksburn, Aberdeen AB2 9SB* and C. H. KNIGHT, *Hannah Research Institute, Ayr KA6 5HL*

The term 'body composition' might be expected to cover all constituents of the body, but for the purpose of the present short review it will be limited to a commonly accepted usage, namely the amount or proportion of fat on the body as compared with the lean tissue mass.

A number of non-invasive methods are available for measurement of body fat, using either chemical or physical characteristics of tissues. Of these only four will be discussed, neutron-activation analysis (NAA), ultrasound, X-ray computed tomography (CT) and nuclear magnetic resonance (NMR) imaging, with the greatest emphasis being placed on this latter, recently introduced technique.

NAA

NAA works by changing some stable isotopes of body elements into radioactive ones. This is achieved by bombarding the body with neutrons, some of which 'hit' nuclei which are able to capture them. These nuclei become unstable and release energy or particles, or both, to attain a stable state. In most cases these emissions are observed directly, although sometimes activation is observed at second hand due to the effects of the emissions on other atoms.

Neutrons can be produced by devices such as a van der Graaf generator, linear accelerator, cyclotron, etc. The nature of the generator, the particle accelerated and the target at which the particle is aimed determines the energy of the resultant neutron. The amount of radioactivity produced in the sample (e.g. the body) is determined by a variety of factors including:

(a) *Fixed factors*: (1) cross section, the probability that a neutron will interact with a nucleus; (2) decay constant, the time it takes for the activated nucleus to decay (see Table 1); (3) isotopic abundance, the amount of the nucleus present in the body.

(b) *Operator-controlled factors*: (1) irradiation time, there is a build-up of radioactivity from non-prompt decaying nuclei; (2) sample size, the number of suitable nuclei available; (3) neutron flux, the number of neutrons available in a given period.

The type of nucleus which is affected by the neutron, the nuclear reaction it undergoes and the nature of the emission are determined by the energy of the incident neutron. On receiving a low-energy neutron the absorbing nucleus will normally respond by releasing a gamma, hence hydrogen becomes deuterium or ^{14}N becomes ^{15}N. In each case a gamma of specific energy is emitted at the time of absorption of the neutron, hence irradiation and detection must be virtually simultaneous using equipment similar to that shown in Fig. 1.

A system for the detection of prompt gammas provides a spectrum of gamma energies in which individual peaks originate from different activated nuclei in the sample. In Fig. 2 a gamma spectrum from the whole human is shown (from Kehayias *et al.* 1986) in which the peaks (MeV) are: 2·23 gamma from H, 4·44 gamma from carbon, 6·1 gamma from oxygen.

https://doi.org/10.1079/PNS19880056 Published online by Cambridge University Press

Table 1. *Examples of neutron-activation reactions which can occur involving biologically important atomic species*

Absorber	(Input, Output)	Product	Half-life
^{1}H	(n,γ)	^{2}H	Prompt
$^{12}C^{*}$	(n,n′)	^{12}C	Prompt
^{12}C	(n,γ)	^{13}C	Prompt
^{14}N	(n,γ)	^{15}N	Prompt
^{14}N	(n,2n)	^{13}N	9·96 min (e^{+})
$^{16}O^{*}$	(n,n′)	^{16}O	Prompt
^{16}O	(n,γ)	^{17}O	Prompt
^{16}O	(n,p)	^{16}N	7·2 s

n, neutron; p, proton; e^{+}, positron.
*Inelastic scattering during which a gamma is released.

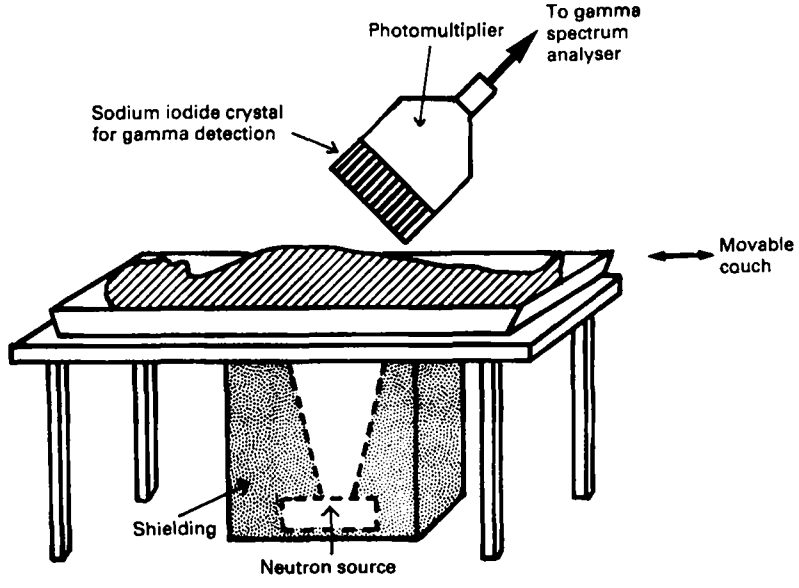

Fig. 1. Simplified apparatus for neutron-activation analysis.

Table 2. *Total body nitrogen (TBN), chlorine (TBCl) and fat (TBFat) in two cadavers measured by neutron-activation (NAA) and chemical analysis (Chem) (from Beddoe* et al. *1986)*

(Mean values with their standard errors)

		TBN (kg)		TBCl (kg)		TBFat (kg)	
Subject		Mean	SE	Mean	SE	Mean	SE
Cadaver 1	NAA	1·47	0·02	0·144	0·004	10·71	0·13
	Chem	1·51	0·03	0·147	0·002	10·48	0·15
Cadaver 2	NAA	0·576	0·008	0·0227	0·0017	6·77	0·05
	Chem	0·572	0·014	0·0250	0·0014	7·71	0·17

https://doi.org/10.1079/PNS19880056 Published online by Cambridge University Press

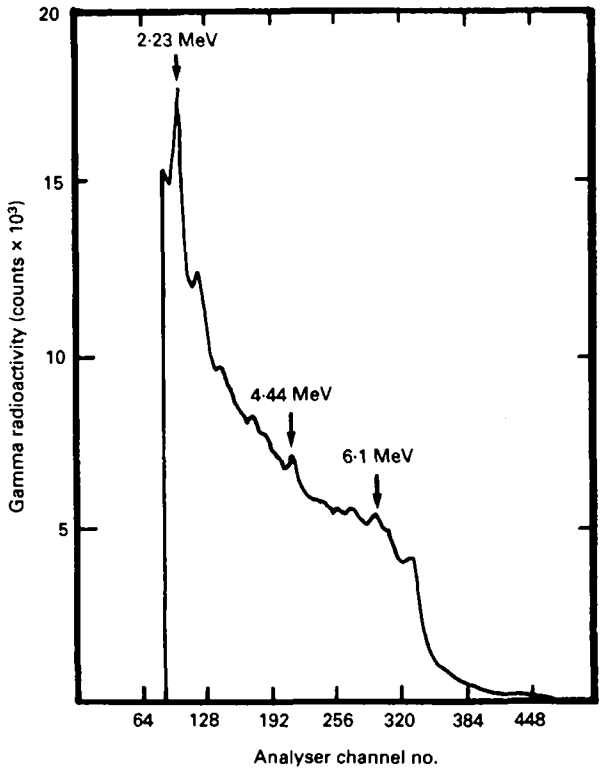

Fig. 2. Neutron-activation-analysis-induced gamma-ray spectrum from a normal human being. From Kehayias *et al.* (1986).

Comparison of peak sizes with those obtained by irradiating a standard source gives the elemental composition of the absorbing body, as shown in Table 2 (from Beddoe *et al.* (1986)). Body fat content is estimated from the spectra because of the very high C content (77%) of lipids.

If high-energy neutrons are used, absorbing nuclei tend to disintegrate, releasing nuclear particles. For example, ^{14}N can absorb a high-energy neutron and release two neutrons to become ^{13}N. ^{13}N is unstable and in turn decays, releasing a positron. This loses its energy and contacts with a normal electron causing mutual anihilation with the release of two gammas of equal energy at 180° to each other. Since the ^{13}N has (in NAA terms) a long half-life of nearly 10 min, irradiation and counting do not need to be simultaneous. This is advantageous if information about spatial distribution of activated nuclei is required.

Sophisticated imaging methods such as positron-emission tomography can provide spatial information about the distribution of positron-emitting isotopes. A ring of detectors is placed round the sample. Two detectors will be affected by the anihilation gammas of the e^+/e^- interaction and a pulse is recorded only when two detectors are stimulated, hence reducing noise from single events such as decays of non-positron-emitting isotopes, cosmic radiation, etc. The anihilation occurs on the straight line between the two detectors because the gammas come out at 180° to each other. When enough pulses have been registered from the sample, all the straight lines can be computed together into an image of distribution of the decaying isotope.

Table 3. *Velocity and attenuation of ultrasound in tissues*

Material	Ultrasound velocity (/ms)	Ultrasound attenuation coefficient at 1 MHz (dB/cm)
Air	330	10
Bone	2700–4100	3–10
Muscle	1545–1630	1·5–2·5
Soft tissue (except muscle)	1460–1615	0·3–1·5
Water	1480	0·0002

Ultrasound

As its name implies, ultrasound is a sonic vibration at a frequency above that of human ear response. For imaging, the frequencing range is 1–15 MHz. Sound waves penetrate tissues and differences in tissue composition alter both velocity of travel and attenuation of the ultrasound (Table 3).

Sound waves are reflected by boundaries between tissues or by boundaries between tissue and air or liquid. The amount of reflection is fairly characteristic for a given interface (Table 4). Fat–tissue boundaries tend to be strong reflectors. The reflected sound may be monitored and an image produced of spatial distribution of tissues through which the sound wave has passed and the boundaries from which it has been reflected. The classic use of reflected ultrasound is in examination of the fetus *in utero*. The amount of sound actually reflected is low so sound waves transmitted through the tissue may also be monitored. Tissues have characteristic sound absorbing properties so comparison of the input and emitted sound provides information about tissue types.

Ultrasound has been used routinely since the early 1970s for obtaining measurements of fat-layer thickness in body regions. Usually a reflection image is obtained on which fat layers can be seen and measured. Alternatively the speed of the ultrasound can be measured at specific points, e.g. across the rump of a cow. It has been found that a strong relation exists between ultrasound speed in the living animal and amount of adipose tissue in the beef side observed after slaughter (Fig. 3 from Miles *et al.* 1984).

Table 4. *Reflection of longitudinal waves normally incident on the plane boundary between two tissues, expressed in decibels below the level from a perfect reflector*

Tissue interface	dB
Fat–kidney	22
Fat–liver	21
Fat–muscle	20
Fat–spleen	21
Kidney–liver	41
Kidney–muscle	32
Kidney–spleen	45
Liver–muscle	37
Liver–spleen	50
Muscle–skull bone	38
Muscle–spleen	35

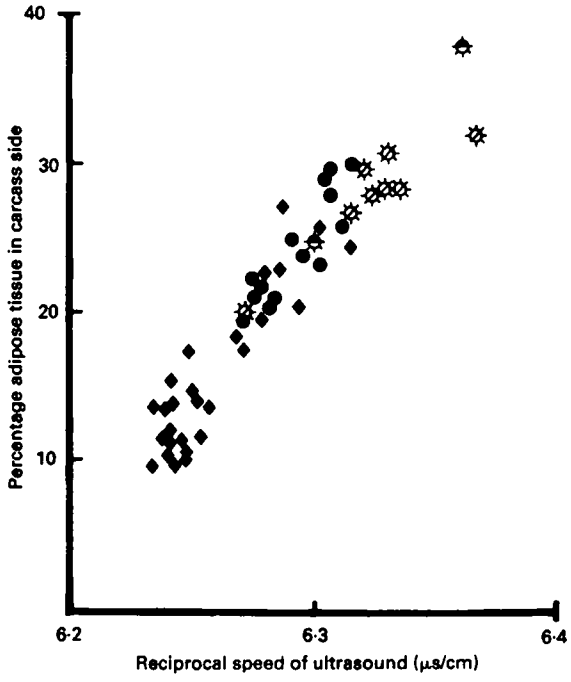

Fig. 3. Correlation between ultrasound speed in cattle hind-limb and proportion of adipose tissue in carcass (values from Miles *et al.* (1984)). (◆), Friesian heifer; (●), Friesian cow; (✡), Hereford heifer; (✡), Hereford cow.

X-ray CT

Tomography means drawing a slice, from the Greek root 'tomo'. If you take a conventional X-ray through the body onto the plate, you produce a shadowgraph in which all penetrated tissues contribute to attenuation in proportion to their thickness and X-ray absorption properties. This is of limited use in assessment of tissue content since definition between soft tissues is poor. To improve soft-tissue contrast a thin slice must be isolated from the rest of the body on which each tissue type is delineated. This is provided by X-ray CT.

X-ray CT produces an image from a series of linear projections of X-ray opacity along strips through the sample. A computational technique called projection reconstruction is used to form the image from these projections. Each projection is obtained by placing the body in a movable X-ray unit (Fig. 4). On one side of the body is the X-ray generator and on the other, in modern equipment, an array of detectors. (One detector alone will produce an image with a poor signal:noise ratio.) This generator–detector assembly is moved in a straight line past the sample. The detector(s) will, therefore, get a large X-ray input when there is no intervening body, but this decreases as the assembly passes over the body where the amount of X-ray reaching the detector will depend on the total amount of absorption through the body at the place being examined at any moment in time. The end result, therefore, will be a plot of X-ray absorbance v. position on the line along the body followed by the assembly. This is one projection. To obtain a second projection the assembly is rotated a small amount (normally 1°) round the sample and again moved over the sample. In most cases this is repeated 180 times round the sample. The information contained in these projections is then assembled to obtain an image of a slice through the body.

https://doi.org/10.1079/PNS19880056 Published online by Cambridge University Press

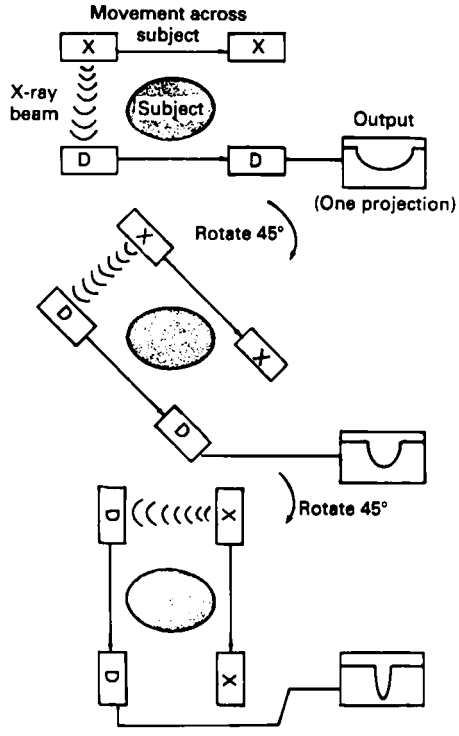

Fig. 4. Illustration of operation of X-ray computed tomography unit. X, X-ray tube; D, detector (or array in modern equipment). These move together across the subject, represented by two spheres of X-ray semi-opaque material. The output from each pass (projection) is shown.

When quantitative measurements are required from an X-ray CT picture the total range of X-ray absorbance is divided into 2000 units (Hounsfield numbers after the inventor of the technique). The scale is centred on the X-ray absorbance of water (given the value zero) with dense bone being +1000 and air being −1000. Soft tissues occupy only a small part of this range (see Fig. 5) but sufficient to allow discrimination. Fat has a low X-ray absorbance and hence is distinguished from other tissues.

Most attempts to use X-ray CT in body composition studies have assessed the proportion of the image units (pixels) in a specific Hounsfield number range, e.g. Sehested (1984) examined sections through the lower abdomen of fat and lean sheep by X-ray CT during life, and by dissection and chemical analysis after slaughter. The X-ray CT images were analysed by drawing a limiting line round the outer edge of the carcass on the image and noting the Hounsfield number of each pixel within this boundary, plotting distribution frequency as a histogram (Fig. 6(*a*)). This method offered possibilities for direct comparison of sections at the same level from different animals, hence a difference plot such as that in Fig. 6(*b*) could be obtained by subtraction of the histogram of a lean animal from that of a fat animal. It can be seen that, in addition to the greater number of pixels in fatty areas (Hounsfield number about −80) there are marked differences in the 'wet' tissue regions. Similar work is being done on pigs by Skjervold *et al.* (1981) and Standal (1984).

https://doi.org/10.1079/PNS19880056 Published online by Cambridge University Press

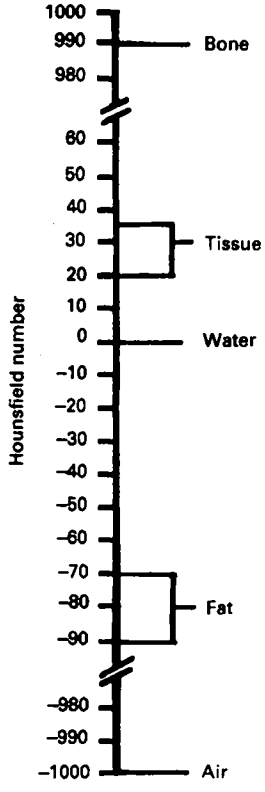

Fig. 5. Hounsfield number scale used for quantification of X-ray computed tomographic images.

Each pixel represents a specific volume within the body. (When the slice thickness is considered as well as the surface plane dimensions the image unit is normally termed a voxel.) Hence from the image it is possible to calculate the volume of visible tissues from X-ray CT images. This has been done, for example, by Sorensen (1984) who followed the variation in volume of adipose tissue in four goats during pregnancy and lactation (Fig. 7).

NMR imaging

NMR imaging, like the X-ray method discussed previously, is a CT technique, although the method of image production and the information in it is completely different. NMR allows observation of the property of spin exhibited by certain nuclei. For the present purpose the nucleus of interest is the H-proton which has a nuclear spin of 1/2. Spin gives the nucleus a magnetic moment and it will, therefore, align with an external magnetic field. Both parallel and anti-parallel alignment is possible with an energy difference between them, and this energy difference is exploited to yield the NMR signal.

https://doi.org/10.1079/PNS19880056 Published online by Cambridge University Press

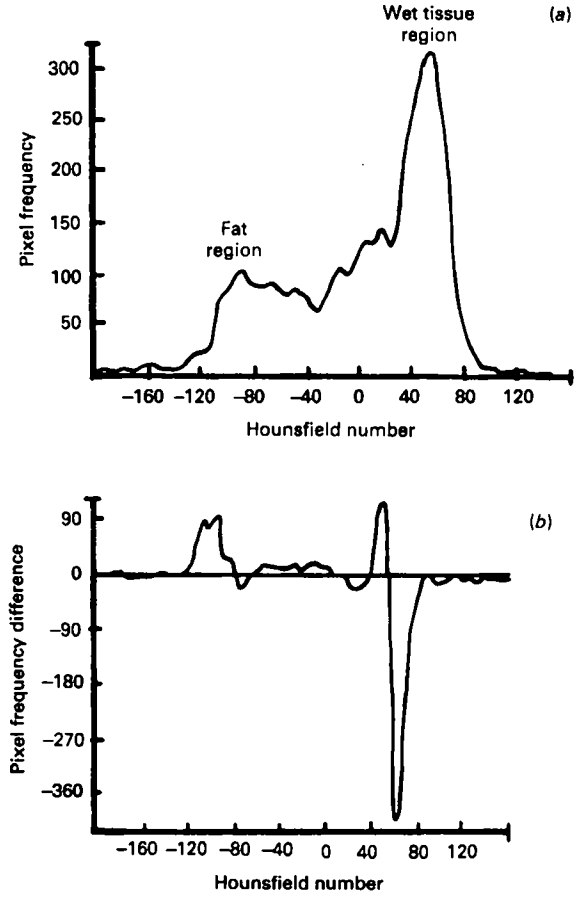

Fig. 6. (*a*) Distribution frequency of Hounsfield numbers within a defined outline in an X-ray computed tomographic image taken at the 4th lumbar vertebra of a sheep. (*b*) Difference between histograms from fat and lean sheep. Parts (*a*) and (*b*) redrawn from Sehested (1984).

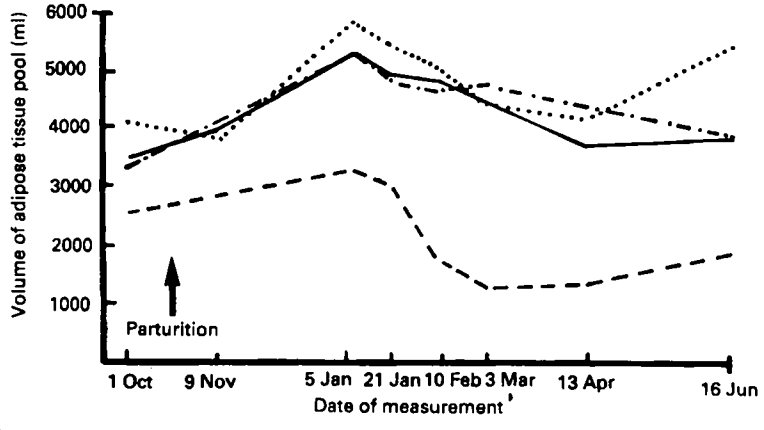

Fig. 7. X-ray computed tomography-measured size of the adipose pool of four goats (——, – – –, –·–·–, ····) during pregnancy and laction. Redrawn from Sorensen (1984).

https://doi.org/10.1079/PNS19880056 Published online by Cambridge University Press

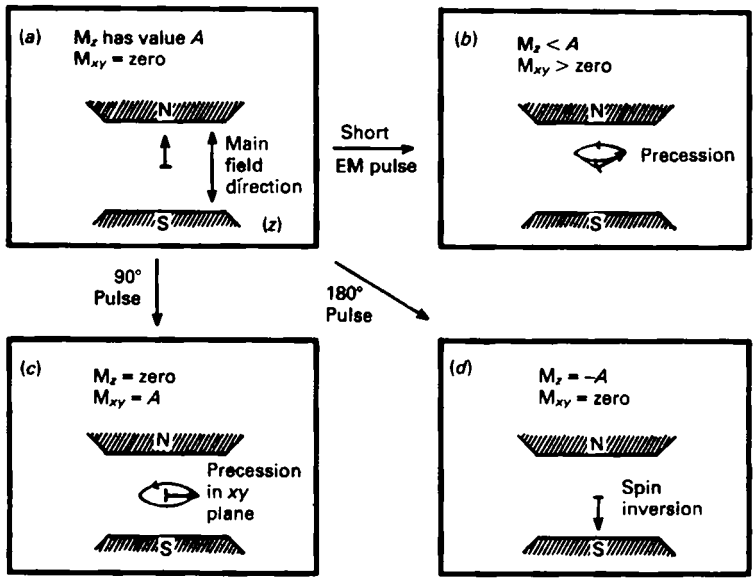

Fig. 8. Effects of radio-wave pulses of varying sizes on the precession angle of the spin magnetization (M) in a nuclear magnetic resonance experiment. EM, Electromagnetic.

If the total proton population in a sample such as water is examined, the difference between the numbers of spins in the two alignments gives a net magnetization whose vector, in the ground state, will be in the low-energy orientation. In effect this magnetization vector can be regarded as precessing round an axis which is the same as the direction of the applied magnetic field, normally termed the z axis, as shown in Fig. 8. There is a simple relation between the precession frequency (f) and the strength of the applied magnetic field (B), given by:

$$\omega = \gamma B,$$

where ω is 2 π multiplied by f and γ is the gyromagnetic ratio, a term containing information about the angular momentum and magnetic moment of the spin. If B is increased f also increases, a vital consideration in NMR imaging.

To interrogate the spin system the alignment of the magnetization vector is altered by subjecting the sample to a pulse of radio waves (RF) at the precession frequency f. As shown in Fig. 8, a small (amplitude or duration) RF pulse will increase the precession angle, a larger pulse (normally termed a 90° pulse) brings the magnetization vector onto the xy plane (at right angles to the direction of the applied magnetic field). Double this amplitude or duration of RF pulse causes inversion of the magnetization vector (a 180° pulse). In standard NMR and NMR imaging, detection is only possible in the x and y directions, hence the initial state. A 180° pulse will not induce an NMR signal, but a signal whose initial amplitude is proportional to the number of NMR-detectable spins in the sample will be induced in the receiver after a 90° pulse.

The RF pulse causes excitation in the sample which is followed by relaxation to the ground state. NMR relaxation takes two forms. Relaxation along the z axis involves excitation energy being dissipated as heat in the matrix of the sample. This is termed spin-lattice relaxation and has a time constant T_1. Loss of NMR signal also occurs

https://doi.org/10.1079/PNS19880056 Published online by Cambridge University Press

through loss of coherence of the spins. This is spin–spin relaxation with a time constant T_2. In NMR imaging both these relaxation processes, as well as the spin population density, are important in providing contrast between tissues.

Spatial information in the NMR image is obtained by applying a controlled magnetic field gradient to the sample. Hence spins in one part of the body have a different f value (and hence respond to a different RF frequency) from those in another region. The techniques for producing and analysing the NMR signal to form the image are complex and beyond the scope of this review. More details can be obtained from Foster & Hutchison (1988).

In the NMR image one observes only protons of small, mobile molecules, hence most NMR signal comes from water. It is, however, possible to 'see' H in triglyceride chains. Although membrane lipids are too constrained to give an NMR signal under imaging conditions, those free in adipose tissue have sufficient mobility (and hence a long enough T_2 value) to be observed, albeit with a very short T_1 value. Tissue water is, to some extent, structured and hence has much shorter relaxation times than free water but the 'wet' tissue T_1 is always longer than that of tissues with high free-lipid contents although T_1 and T_2 vary between tissues.

Since the conditions under which an NMR image is collected (i.e. the pulse sequence) can be varied to alter the extent to which the spin density signal is weighted with T_1 or T_2 information, or both (Plate 1), it is possible to optimize contrast between any pair of tissues, such as fat and muscle, with different relaxation characteristics (Foster *et al.* 1984; Foster, 1986). This has been used, for example, by Knight *et al.* (1984) to measure udder volume in lactating goats, and by Fuller *et al.* (1986) to monitor sites of adipose tissue loss in dieting human females. In both cases NMR sections were taken through appropriate regions of the subjects and area measurements of the tissues made from the images. In the case of Knight *et al.* (1984) these areas were used to obtain organ volume estimates (Plate 2). In an earlier study Fuller *et al.* (1985) showed that area measurements of fat obtained by planimetry of photographs of actual slices through a pig and of photographs of NMR images in the same region taken before death give markedly similar results.

Discussion

All the techniques discussed here have positive abilities in body-composition studies, but they also have disadvantages. Few techniques use the type of mobile, inexpensive and robust equipment which could be used by farmers for monitoring their stock. It is, therefore, unlikely that the more sophisticated techniques will extend beyond research use. On the other hand the detailed information given by, for example, X-ray CT or NMR imaging is not needed for stock rearing, although if simple carcass fat measurements can be obtained on the live animal using, perhaps, ultrasound, these would be useful. At research stations where experimental feeding or breeding programmes may be based on details of fat distribution and, of course, in hospitals and clinics, the greater detail of the imaging techniques is of considerable value.

REFERENCES

Beddoe, A. H., Streat, S. J. & Hill, G. L. (1986). In *In Vivo Body Composition Studies*, pp. 25–32 [K. J. Ellis, S. Yasumura and W. D. Morgan, editors]. London: Institute of Physical Sciences in Medicine.

Foster, M. A. (1986). In *Functional Studies Using NMR*, pp. 147–166 [V. R. McCready, M. Leach and P. J. Ell, editors]. London: Springer-Verlag.

Foster, M. A. & Hutchison, J. M. S. (1988). *Practical NMR Imaging*. Oxford: IRL Press Ltd.

Foster, M. A., Hutchison, J. M. S., Mallard, J. R. & Fuller, M. (1984). *Magnetic Resonance Imaging* **2**, 187–192.

Fuller, M. F., Foster, M. A. & Hutchison, J. M. S. (1985). *Proceedings of the Nutrition Society* **44**, 108A.

Fuller, M. F., Stratton, M. A., Geddes, D., Fowler, P. A. & Foster, M. A. (1986). In *In Vivo Body Composition Studies*, pp. 55–59 [K. J. Ellis, S. Yasumura and W. D. Morgan, editors]. London: Institute of Physical Sciences in Medicine.

Kehayias, J. J., Ellis, K. J., Cohn, S. H., Yasumura, S. & Weinlein, J. H. (1986). In *In Vivo Body Composition Studies*, pp. 427–435 [K. J. Ellis, S. Yasumura and W. D. Morgan, editors]. London: Institute of Physical Sciences in Medicine.

Knight, C. H., Foster, M. A. & Rimmington, J. E. (1984). In *In Vivo Measurement of Body Composition in Meat Animals*, p. 175 [D. Lister, editor]. London: Elsevier.

Miles, C. A., Fursey, G. A. J. & York, R. W. (1984). In *In Vivo Measurement of Body Composition in Meat Animals*, pp. 93–105 [D. Lister, editor]. London: Elsevier.

Sehested, E. (1984). In *In Vivo Measurement of Body Composition in Meat Animals*, pp. 67–74 [D. Lister, editor]. London: Elsevier.

Skjervold, H., Grønseth, K., Vangen, O. & Evensen, A. (1981). *Zeitschrift für Tierzüchtung und Züchtungsbiologie* **98**, 77–79.

Sorensen, M. T. (1984). In *In Vivo Measurement of Body Composition in Meat Animals*, pp. 75–83 [D Lister, editor]. London: Elsevier.

Standal, N. (1984). In *In Vivo Measurement of Body Composition in Meat Animals*, pp. 43–51 [D Lister, editor]. London: Elsevier.

EXPLANATION OF PLATES

Plate 1. Variation in contrast between adipose tissue and muscle in nuclear magnetic resonance images through a pig at the level of the heart. (*a*) Spin density image, (*b*) the T_1-weighted inversion recovery image (where T_1 is the spin-lattice-relaxation time, see p. 383), (*c*) actual body slice at the same level.

Plate 2. Nuclear magnetic resonance images through the udder of a goat (*a*) early and (*b*) late in the first pregnancy.

Printed in Great Britain

https://doi.org/10.1079/PNS19880056 Published online by Cambridge University Press

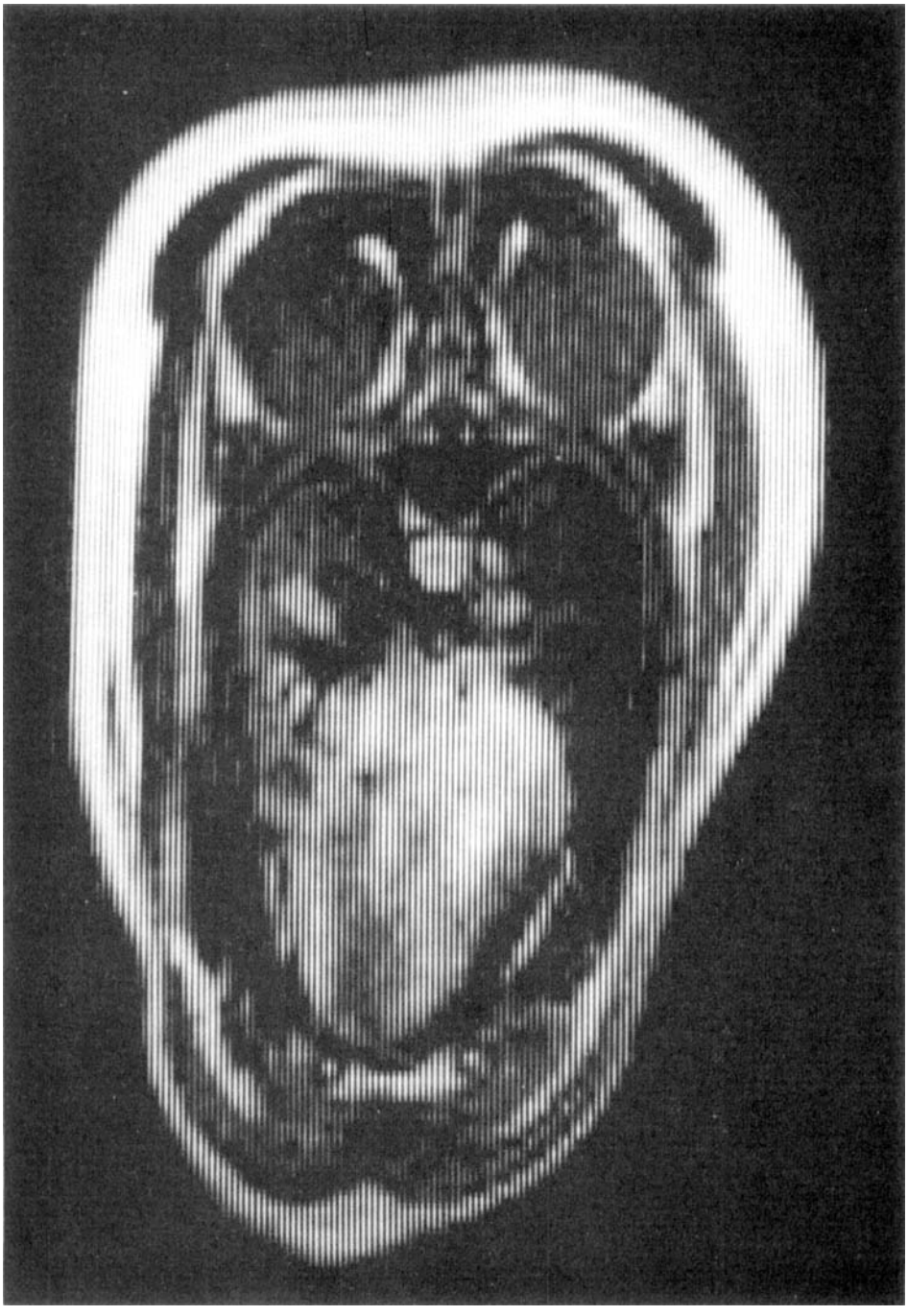

https://doi.org/10.1079/PNS19880056 Published online by Cambridge University Press

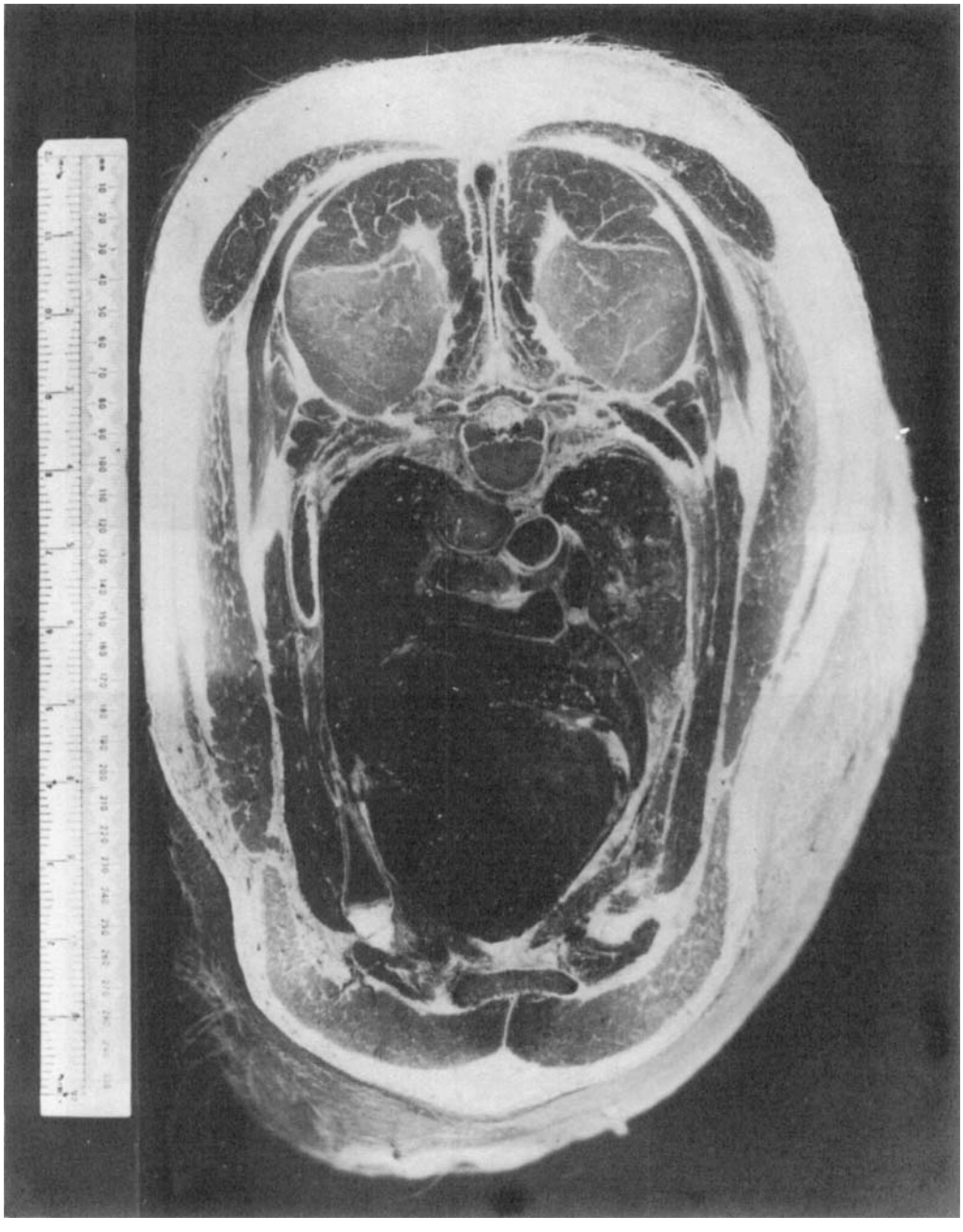

M. A. Foster and others

https://doi.org/10.1079/PNS19880056 Published online by Cambridge University Press

(a)

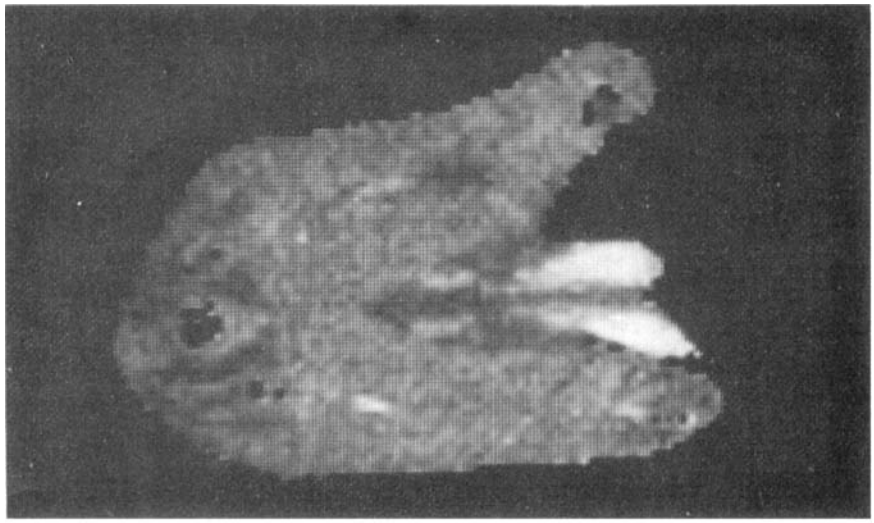

(b)

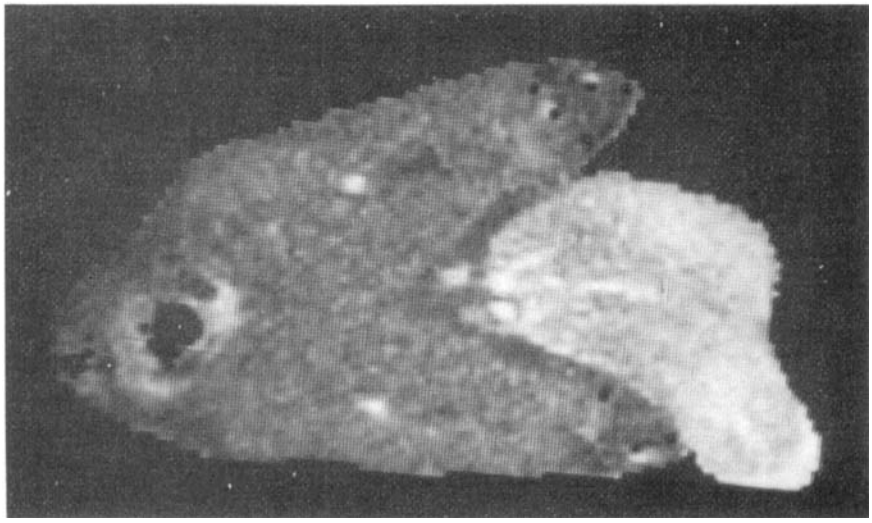

M. A. FOSTER AND OTHERS

https://doi.org/10.1079/PNS19880056 Published online by Cambridge University Press